Development of an iterative Procedure with a Flow Solver for optimizing the Yarn Speed in a Main Nozzle of an Air Jet Loom

Lucas Delcour[a]*, Jozef Peeters[b] and Joris Degroote[a,c]

[a]Department of Flow, Heat and Combustion Mechanics, Faculty of Engineering and Architecture, Ghent University, Ghent, Belgium

[b]Picanol NV, Ieper, Belgium

[c]Flanders Make, Belgium

*lucas.delcour@ugent.be; http://orcid.org/0000-0002-0485-7701

Development of an iterative Procedure with a Flow Solver for optimizing the Yarn Speed in a Main Nozzle of an Air Jet Loom

In this research, a fluid-structure interaction (FSI) framework was established to estimate the velocity of a yarn as it is propelled by the main nozzle. To allow the methodology to be used in an optimization context, the computational time was limited as much as possible. The methodology was first validated on polymer coated yarns to avoid any influence of yarn hairiness. Results from the calculations were compared to experiments and adequate agreement was found without tuning. Subsequently, an extension to hairy yarns was made by representing the hairiness as a wall roughness. The roughness height was determined by matching the simulated to the experimental velocity for a single case. The approach was validated by applying the obtained roughness height to different setups and comparing the simulations to the corresponding experiments. Taking into account some limitations, the methodology can be applied for optimization purposes using either smooth or hairy yarns.

Keywords: computational fluid dynamics; air jet loom; main nozzle; yarn velocity; fluid-structure interaction

Introduction

In air-jet weaving looms the main nozzle is responsible for pulling the yarn from the prewinder and launching it into the reed. To provide sufficient propulsion force to the yarn, high air velocities are required. This is achieved by supplying the main nozzle with highly pressurized air, which expands inside the nozzle, resulting in high velocities and complex flow patterns. The insertion rate that can be achieved is directly dependent on the attainable yarn velocity. This velocity depends mainly on the interaction between the air flow and the yarn.

Air jet weaving looms thrive on their high insertion rates, but suffer from substantial energetic cost. Optimization of the main nozzle could further increase the productivity, while maintaining or even decreasing the endured cost. Experimental optimization is, however, very time and resource-intensive. Furthermore, the complex

flow patterns and yarn-flow interaction render the choice of appropriate parameters less intuitive. Numerical procedures allow the user to perform extensive parameter sweeps or even use optimization algorithms with limited investment. A numerical model which provides the yarn velocity - instead of just the air flow speed or the force on a yarn - can be used to reduce the air consumption while maintaining the same insertion rate or to improve the insertion rate for a certain energy consumption.

The following paragraphs provide an overview of the relevant publications concerning (optimization of) the main nozzle in air jet looms. To clarify some terminology, a modelled section cut of a standard nozzle is shown in Figure 1.

"[Insert Figure 1]"

One of the first investigations into the optimization of the main nozzle was performed by Uno et al. (1961). They experimentally studied different nozzle and tube geometries, which deviate somewhat from the current standard. One of their conclusions was that Laval tubes were unsuited for weft propulsion. However, this statement was revisited by Jeong, Kim, Choi, & Lee (2005), who performed experimental analysis into the effect of acceleration tube diameter and the addition of a suction hole to the acceleration tube. In 1972, Uno (1972) published a paper focused on avoiding the crooked flight of the yarn after exiting the main nozzle. To do so, they investigated the influence of lengthening the acceleration tube. Contrary to the previously mentioned paper (Uno et al., 1961), a non-invasive velocity measurement method was employed. Furthermore, some numerical calculations were performed, using a velocity-dependent force coefficient and assuming a constant air velocity in the tube.

Mohamed and Salama (1986) performed research on a more modern main nozzle configuration. They analyzed experimentally the influence of acceleration tube length, internal yarn tube diameter and yarn tube position on the turbulence and air velocity at

the exit of the nozzle. Adanur and Mohamed (1991, 1992a, 1992b) published a series of papers focused on establishing theoretical models to calculate the yarn's velocity for a single nozzle air-jet filling insertion from measured values of air velocity. To calculate the aerodynamic force on the yarn they relied on experimentally measured force coefficients. Their main focus was on the comparison between drum and loop storage systems. Nosraty, Jedi, & Mousaloo (2008) later on used the model from Adanur and Mohamed as a basis for their own yarn-motion model in a single nozzle air-jet loom. Nosraty et al. (2008) considered several combinations of empirical models for the air flow velocity and force coefficient to simulate the yarn motion (yarn velocity, acceleration and tension). The combination resulting in the best agreement with experiments was then selected for implementation into a simulation tool to establish the most suitable conditions (minimum air supply pressure) for weft insertion.

Ishida and Okajima (1994a, 1994b) published a 2-part paper in which they tried to obtain some basic data for an optimum design of the main nozzle. In the first part, the flow inside the main nozzle was analyzed by measuring static pressure along the acceleration tube and using a 1-dimensional adiabatic approximation to the flow. The flow was analyzed for several tank pressures and acceleration tube lengths with emphasis on choking phenomena in the nozzle. In the second part more attention was devoted to the flow at the exit of the acceleration tube, both in sub- and supersonic cases. They also measured weft drag forces and concluded that increasing the tank pressure beyond the choking point of the end of the acceleration tube is of little use since the drag force only increases slightly and the yarn tends to become unstable due to shock waves.

Oh, Kim, & Song (2001) were among the first to use computational fluid dynamics (CFD) for analysis of the main nozzle. They performed 2D-axisymmetric CFD simulations on a nozzle geometry very similar to that from Ishida and Okajima (1994a,

1994b). As a simplification, they assumed the yarn tube to be closed off. Calculations were performed for a set of acceleration tube lengths and the flow fields were compared. More importantly, however, they investigated the effect of rounding off the nozzle core end and observed a decrease in separation zone length, implying a reduction in total pressure loss. Prabkeao and Aoki (2005) performed some additional experimental research into the influence of the nozzle core shape by considering 7 different configurations with constant throat area. However, no general conclusions about the optimal shape were obtained, which highlights the complexity of optimizing a main nozzle. Two-dimensional, axisymmetric CFD-simulations were also performed by Kim, Lim, Lee, & Chun (2007), with somewhat more focus on the shock trains in the supersonic regime. They, however had to conclude that the employed k-ε turbulence model was not adequate for this purpose. According to their observations, a longer acceleration tube increases the drag force but also increases the total pressure loss in the tube and both factors are to be considered when looking for an optimal design. Belforte, Mattiazo, Viktorov, & Visconte (2009) executed calculations with different turbulence models and compared the calculated force on a stationary yarn (integrated wall shear stress on a rigid cylinder along the axis) to that measured in experiments. He obtained the best agreement by using a standard k-ε turbulence model with non-equilibrium wall functions and used this model to assess the influence of acceleration tube length and angle of divergence. His results showed that small divergence angles are beneficial, as was previously postulated by Jeong et al. (2005).

In 2015 Chen, Feng, Dong, Wang, & Liu (2015) analyzed the flow field inside a standard and a newly designed main nozzle by means of 3-dimensional CFD-simulations. The main goal was to decrease or eliminate the backflow observed at high inlet pressure by considering 2 nozzle cores and air flow inlets. Nozzle designs were compared based

on the calculated centerline velocity and the force on the yarn, calculated using a fixed force coefficient. Three-dimensional CFD-simulations were also executed by Jin, Cui, Zhu, Lin, & Hu (2016), who proposed to incline the nozzle core end in order to improve mixing between the high speed nozzle flow and the low speed flow from the yarn tube. They also analyzed the flow for 2 different yarn tube diameters. Concepts were evaluated according to the velocity on the axis, flow line pattern and turbulence intensity. Using 3-dimensional CFD-simulations, Lan, Liu, & Feng (2017) performed an optimization of the main nozzle considering 5 parameters and 4 levels for each parameter. Sixteen numerical simulations were performed based on a 2-(4,5,1) orthogonal array. The simulations did not include a structure representing the yarn. Different configurations were evaluated based on nozzle exit velocity and static weft drag force. The drag force was obtained by using a fixed force coefficient. In the yarn tube and the expansion region the flow velocity was extracted from the simulations; in the acceleration tube, Fanno flow was assumed for the calculation of the drag force.

Another main nozzle optimization, using CFD, was done by Osman (2017). The CFD calculations were 2D-axisymmetric and the geometry included a stationary cylinder on the axis. Fifteen parameters were considered. For the optimization procedure an interior-point algorithm was used. The force on the central cylinder, obtained by integration of the calculated wall shear stress, was used as objective function with a penalization for geometries subjected to backflow in the yarn tube. Simulations were performed with 2 different yarn diameters. Osman et al. (2017) also developed a fluid-structure interaction (FSI) framework using a 2D flow simulation with a 3D structural model to simulate the 3D yarn motion inside the main nozzle. The methodology is capable of predicting the yarn velocity quite well, but simulations require about 36 hours of calculation time on a single core (of a 12-core Intel Xeon E5-2680v3 2.5 GHz CPU),

which limits the usability in an optimization context. Furthermore, force coefficients need to be tuned. Wu, Chen, Liu, & Hu (2016) also performed FSI-simulations, focusing on the whipping behavior of the part of the yarn protruding from the main nozzle. Their simulations were performed on a 2D-planar geometry without axial motion of the yarn.

As can be seen from the above overview, optimization of the main nozzle was initially based on extensive experimental trials. Nowadays, one can consider using numerical procedures supported by some experiments to perform more thorough optimization. The previous works using CFD as part of their optimization, either optimize the geometry by looking at the flow patterns (flow lines, turbulence intensity, centerline velocity, …) or calculating the force on a static yarn either through the use of a force coefficient or integration of the calculated wall shear stress or on a moving yarn using force coefficients. No papers have been found documenting a methodology in which the yarn velocity is calculated in a fast way such that it is suitable for optimization. In this paper, an FSI-methodology with 2-way coupling is suggested to quickly calculate the regime velocity of a yarn as it is propelled by the main nozzle. The force on the yarn is obtained by integration of the wall shear stress on a moving yarn. At first smooth yarns are considered to avoid the influence of the yarn's surface texture. Later on, hairy yarns are also considered and an attempt is made to model the yarn's surface texture as an equivalent wall roughness height. By directly calculating the velocity of the yarn, the possibility originates of using the yarn velocity directly as an objective or constraint for an optimization problem. For example, one could put forward a desired increase in production speed and link it to the required increase of yarn speed. The yarn speed predominantly depends on the air flow generated by the main nozzle. Accordingly, a parametrization of the nozzle geometry combined with a parameter sweep can provide an idea about what parameters to consider and the achievable gain in terms of yarn speed by

geometric variations. If the desired improvement cannot be attained by simple geometric variations, one could also consider augmenting the inlet pressure and evaluating the increase in operational costs that accompany it. As the model is fast, it is also suitable for uncertainty quantification (UQ), such that the statistical distribution of parameters calculated in the simulation (e.g. yarn speed) as a function of the distribution of input parameters (e.g. lengths, angles) due to production variations can be obtained."

Methodology

Numerical setup

As was mentioned previously, the goal of this work is to obtain the yarn velocity from numerical simulation. To this end a structural model and a flow model are combined. Both models are chosen to allow for a fast calculation while remaining sufficiently accurate to predict the correct data trends. For validation, the results from the simulations will be compared to experimental results obtained from the setup described further.

A 2D, axisymmetric model is employed; the thread is represented by a rigid cylinder centered on the axis, extending over the entire domain. A moving-wall boundary condition is assigned to this cylinder; the velocity is calculated from the interaction with the air and the structural boundary conditions applied to the yarn.

In general fluid-structure interaction simulations found in literature, the structural motion is calculated using a finite element analysis (FEA). The influence of the structure on the fluid is then included by deforming the fluid grid or immersed boundary or similar techniques. As the yarn is constrained to move axially as a rigid body in this work, the effect of the structure on the flow can completely be taken into account by a moving wall boundary condition, which essentially imposes an axial velocity component to the flow at the yarn wall.

A sketch of an example geometry can be found in Figure 2 and Figure 3 displays the corresponding mesh. A flow chart of the general process is depicted in Figure 4.

"[Insert Figure 2]"

"[Insert Figure 3]"

"[Insert Figure 4]"

The fundamental concept is as follows. The yarn velocity is imposed on the cylinder wall in the flow solver, which calculates the steady state flow (A) and extracts, from this, the aerodynamic force on the yarn by integrating the wall shear stress (no force coefficient involved) (B). The structural solver then uses this force as input and combines it with the calculated yarn withdrawal force to determine the force balance (C). Subsequently, the obtained force imbalance is used to obtain an updated velocity (D). This process is repeated until the force imbalance drops below a specified threshold.

As the regime velocity of the yarn is of interest, there is no need to calculate the entire transient behavior of the yarn and, thus, steady state calculations can be performed. Unless otherwise mentioned, the flow solver is configured as described next. Second order upwind schemes are used for the convective terms in the density, momentum and energy equations. Furthermore, the k-ω SST model is used as turbulence model as this has proven adequate in previous research (Osman, 2017, Osman et al., 2017). For the calculations, a single value for the pressure has to be imposed at the pressure inlet, the flow is then initialized and solved using a pseudo-transient approach to avoid divergence. For air the ideal gas law is employed. The flow calculations are performed using Ansys Fluent 17.2 (Ansys Inc.).

The physical structure considered is a yarn. In the model it is represented by a rigid cylinder, centered on the axis of the nozzle. The cylinder is only allowed to move in the axial direction. Two forces are considered to be acting on the yarn: an aerodynamic

force, resulting from the surrounding air flow and a tension force, required for accelerating a new section of the yarn from zero velocity to the current yarn velocity.

In the experimental setup (described later on) the main nozzle is solely responsible for propulsion of the yarn. Within the main nozzle the yarn is confined by the nozzle itself, although radial oscillations of the yarn do occur, these do not substantially affect the overall axial force on the yarn. When outside the main nozzle the yarn is still tensioned by the main nozzle jet and maintains a rather straight position. Further away from the main nozzle exit the flow speed quickly diminishes and its contribution to the overall axial force drops off fast. Therefore, it can be concluded that for the purpose of calculating the axial velocity of the yarn, the yarn can be considered as a rigid cylinder along the centerline. This hypothesis is also confirmed by a good agreement between simulation and experiments.

The experimental setup is designed to minimize yarn ballooning (by careful preparation of the windings) and friction in the guide eye (by using a smooth polymer lining), therefore, these forces can be neglected in the structural model. Furthermore, gravity is not considered since this has no horizontal component. A sketch of the structural model with the relevant forces is provided in Figure 5.

"[Insert Figure 5]"

An expression for the yarn withdrawal force T can be derived from a momentum balance. If the yarn is moving at a uniform velocity u_d and accelerates a stationary piece of yarn, then the momentum-increase in a timestep Δt corresponds to:

$$\Delta P = \Delta m \cdot u_d = (\rho_A \cdot u_d \cdot \Delta t) \cdot u_d \qquad (1)$$

with ρ_A the linear density of the yarn expressed in [kg⁄m]. By considering infinitesimally small timesteps an expression for the instantaneous tension force is obtained:

$$\lim_{\Delta t \to 0}\left(\frac{\Delta P}{\Delta t}\right) = \frac{dP}{dt} = T = \rho_A \cdot u_d^2 \quad (2)$$

The aerodynamic force

In general there are two distinct methods of obtaining the aerodynamic force on a yarn subjected to an axial flow. One possibility is to rely on experimentally tuned friction coefficients (C_f) and a functional relationship of the form $\frac{1}{2} \cdot \rho \cdot v^2 \cdot A \cdot C_f$, with ρ the density of the fluid, A the wet surface area and v a velocity measure of the flow relative to the yarn speed. One of the main drawbacks of this method is that it requires meticulously executed experiments to determine the friction coefficient. Especially, since the friction coefficient varies with the relative velocity of the yarn with respect to the flow (Szabó, Patkó, & Oroszlány, 2010). Furthermore, the velocity measure to be used is not uniquely defined and the friction coefficient can strongly depend on the nozzle geometry and the yarn texture (Adanur and Turel, 2004).

Another possibility is to rely on, the more fundamental, boundary layer theory. This is also the approach opted for in the current research. The viscous force exerted by the flow on the wall in fact results from the wall imposing its velocity to the fluid at the contact region (no-slip boundary condition). This creates a velocity gradient in the fluid which, in combination with the fluid's viscosity, results in a tractional force. Figure 6 displays the calculated velocity magnitude for a specific case. The two top figures provide a zoomed in version of the flow field, with the shaded area representing the yarn. In the bottom two figures the velocity magnitude along the vertical lines, drawn on the contour plots, are shown. One can clearly observe the presence of a velocity gradient, responsible for the aerodynamic force exerted on the yarn. On the yarn wall the fluid moves at the same velocity as the yarn (in this case 34.4 m/s), due to the no-slip boundary condition in the flow calculation.

"[Insert Figure 6]"

The interaction between a fluid and a no-slip wall is described by boundary layer theory. Generally, the flow near a wall obeys the following self-similar laws:

$$u^+ = y^+ \text{ ; for } y^+ < 5 \text{ [viscous sublayer]} \tag{3}$$

$$u^+ = \frac{1}{\kappa}\ln(y^+) + C^+ \text{ ; for } 30 < y^+ \text{[log-law region]} \tag{4}$$

With:

$$y^+ = (y \cdot \sqrt{\frac{\tau_w}{\rho}})/\nu \tag{5}$$

$$u^+ = u/\sqrt{\frac{\tau_w}{\rho}} \tag{6}$$

In these formulas ρ is the fluid density, ν is the fluid's kinematic viscosity, y is the distance from the considered point to the wall (wall distance) and u is the flow velocity in this point. If the wall is moving then u is the relative velocity of the flow with respect to the wall. τ_w is the wall shear stress and, thus, represents the force per unit area exerted by the flow on the wall.

Values of y^+ in between 5 and 30 are best avoided in simulations as they are located between the clearly defined viscous sublayer and log-law region but are, generally, overcome by blending functions. Formulas (3) and (4) and their blending describe a relationship between the cell wall distance, the flow velocity in the wall adjacent cell and the wall shear stress. For a specific case, the cell wall distance is fixed by the mesh; the formulas can, therefore, be reinterpreted as a relationship between the wall shear stress and the velocity in the wall adjacent cell. These formulas, thus, function as a boundary condition to the momentum equations.

Since, in the current research the wall of the central cylinder is considered to be moving, the velocity used in the above relationships is the flow velocity in the wall adjacent cell minus the velocity of the wall. Consequently, the yarn velocity directly influences the flow equations and, hence, the flow (Step A in Figure 4). The yarn velocity is not fixed but is determined based on the wall shear stress obtained from the flow solver. As such a two-way coupling is obtained between the simple structural model and the flow model.

The yarn's surface texture can, however, strongly influence the interaction between the flow and the yarn (Adanur and Turel, 2004). Due to the absence of notable texture for smooth yarns, such as monofilament nylon and polymer coated yarns, the standard boundary layer theory can be used. Conversely, this theory cannot take into account the effects of the surface texture for hairy and multifilament yarns. In this research an attempt is made to model the surface texture by an imposed roughness height. The concept of wall roughness is best known from the Moody diagram (Moody, 1944) which gives the friction factor for internal flow in pipes as a function of the Reynolds number and a non-dimensional roughness height. In the current research, a wall roughness is imposed on the central cylinder, representing the yarn, to artificially increase the calculated wall shear stress. More details on how the roughness height is determined and how it is incorporated into the boundary layer theory will be provided later on.

After determining the wall shear stress in the flow solver, the force on the yarn is obtained by integrating over the entire axial length of the domain (Step B in Figure 4). This is an approximation of reality. The force exerted by the flow on the yarn diminishes as the distance to the nozzle exit increases. From a certain distance onwards this fluid force will not be strong enough anymore to uphold the horizontal position of the yarn as gravitational effects become more important. As a result, the yarn starts deviating from

the centerline and falls towards a zone with lower velocities and thus lower fluid forces, while in the simulations the yarn is assumed to be located on the axis along the entire length of the considered fluid domain. If the distance at which the yarn drops out of the jet falls within the fluid domain considered for the flow calculations, then the distance over which the calculated force is integrated is actually somewhat too long. However, the yarn will only drop out of the jet flow if the flow velocity becomes rather low. This implies that the error endured by the superfluous integration length will be small. It could also be that towards the end of the domain, the yarn velocity exceeds the velocity of the surrounding air. This would mean that the yarn section is compressed. In reality, the yarn is very flexible and this compressive force would have negligible impact on the velocity of previous yarn sections. In the simulation, the yarn is considered as a rigid body and the compressive force is taken into account in the force balance, thus affecting the calculated yarn velocity. The latter effect will be investigated by performing calculations with an axially enlarged domain.

Experimental setup

An experimental setup, using a high-speed camera to record the motion of a thread as it is launched by the main nozzle, has been constructed by Picanol NV (Ieper, Belgium). The camera used was a Kodak Ekta Pro EM. A schematic representation of the setup can be found in Figure 7.

"[Insert Figure 7]"

The experiments are performed using 3 main nozzles. The nozzles are constructed by combining an inlet and a tube section, for which a select number of geometries are available. Two of the nozzles consist of a conical inlet and conical tube section. These will be referred to as CON1 and CON2. Compared to CON1, the inlet and tube section of CON2 have a more pronounced conical shape. The third type of nozzle is composed

of a cylindrical inlet and a cylindrical tube section, it will be referred to as CYL1. An illustrative sketch of the nozzle types can be found in Figure 8. The conical shape is exaggerated for clarity purposes.

"[Insert Figure 8]"

As can be seen in Figure 8 the converging section of the CON1 and CON2 nozzle are constructed from 2 concentric conical walls. The smallest cross section (throat area) is attained right before a dump diffusion into the acceleration tube. Additional geometrical details on the conical nozzles are provided in Table 1.

"[Insert Table 1]"

The yarn is initially stored in the yarn supply device. In front of the main nozzle a sensor (Meggitt model 8530B) is placed to monitor the inlet pressure. The pressure of the 5-liter air reservoir can be altered; for the experiments it was set to 3 bar or 5 bar gauge pressure. The 2/2-valve is electrically controlled; the same signal is used to trigger the high speed camera and the pressure sensor. The recordings of the pressure sensor are used to calculate the input for the CFD-model.

The experiments were performed with 2 types of yarn: a lightweight, monofilament polyester yarn coated with polymer (PVC) and a standard cotton yarn. Close up pictures of these yarns can be found in Figure 9.

"[Insert Figure 9]"

Evenly spaced black dots are applied to the yarns for an estimation of the yarn velocity by analyzing the high-speed videos, recorded at a rate of 10 000 frames per second. The polymer coated yarn has an average density of 76 tex (g/km) and an average diameter of 0.21 mm, the cotton yarn weighs, on average, 100 tex. To provide more accurate data for the simulations, the transported yarn section is weighed after each experiment.

Experiments

In total 12 experiments (4 per nozzle) were executed. For every nozzle, a cotton yarn and a polymer coated yarn were launched with the tank pressure set to 5 bar and 3 bar gauge pressure. The inlet pressure during the launch was measured and the high speed camera recorded the yarn motion in the region between the yarn supply and the nozzle entrance. The high speed videos (10 000 fps) could then be analyzed frame by frame to extract the yarn velocity. For the calculations 2 inputs are of importance, a single value for the inlet pressure and the linear density of the yarn. The average plateau pressure is obtained by taking the maximum of the measured profile and averaging over the pressure values within a 3%-range of that maximum. A typical pressure profile is shown in Figure 10, the dotted lines indicate the accompanying averaging interval.

"[Insert Figure 10]"

Due to the frame rate limit on the camera and the fact that the markings on the yarn have to be distinguishable in the footage, only a limited amount of velocity data points is available and the measurements show quite some fluctuations. The time over which velocity measurements could be taken depends on the yarn velocity and the yarn length that could be stored in the supply device. A different winding had to be used for the cotton yarn due to its low rigidity. As a result, the available yarn length for cotton is much smaller than that for the polymer coated yarns. Due to this and the fluctuations on the measurements, defining an interval for calculating the regime velocity is somewhat subjective. Figure 11 shows the selected intervals for the different experiments. The observed ranges and values are listed in Table 2 and 3. An estimate of the error on the average velocity is also included in the tables. Two contributions for the error are considered. Firstly, it is reasonable to assume that the frame number corresponding to the passing of the first and final dot within the averaging interval are both subjected to a

human error of ±1 frame. This corresponds to an error on the time interval of 2e-5s. The relative error on the time (RE_{time}) then corresponds to:

$$RE_{time} = \pm \frac{2 \cdot 10^{-5}[s]}{\Delta t} \quad (7)$$

in which Δt represents the averaging interval. Secondly, the dots need to have a finite width to be distinguishable on the camera. On average the dots are 0.5 cm long. The length of the dots can be expected to be within a ±50% interval. This can cause an error of 0.5 cm on the recorded distance within the averaging interval. The relative error on the distance (RE_{dist}) is then given by the following formula:

$$RE_{dist} = \pm \frac{0.005\ [m]}{\text{dist}} \quad (8)$$

where $dist$ corresponds to the distance travelled by the yarn during this interval. The absolute error on the velocity (AE_{vel}) then follows from:

$$AE_{vel} = (RE_{dist} + RE_{time}) * dist/\Delta t \quad (9)$$

The results are listed in Table 2 and 3.

"[Insert Figure 11]"

"[Insert Table 2]"

"[Insert Table 3]"

Numerical sensitivity

As the goal is to design a methodology suited for the use in an optimization framework, the calculation time should be sufficiently small. Therefore, the choice was made to employ 2D-models with steady state flow calculations. Some additional numerical parameters such as mesh size, axial domain length and residual level can also influence

the results and affect the observed trend. Their influence is briefly discussed in this section.

For the mesh sensitivity a grid refinement study was performed on the CON1 nozzle at approximately 5 bar overpressure, as this configuration will lead to the highest velocities. The mesh was refined uniformly in both x- and y-direction. The results are tabulated in Table 4.

"[Insert Table 4]"

From the table it can be observed that the solution is not completely mesh independent with remaining differences up to 1% between the meshes. Analysis of pressure and velocity contours confirm that the cells in the coarser meshes are too large to accurately resolve the shock patterns. Nevertheless, the influence of this inaccuracy on the calculated yarn velocity is quite limited (< 1%). Since increasing the number of cells also increases the computational time and the deviations are quite limited, a mesh with approximately 10 000 cells is deemed acceptable. Furthermore, it was verified by simulating the flow over a plate, that the obtained wall shear stress in the k-ω SST is not entirely y^+-independent, unless one resolves the boundary layer. Although the relative differences are acceptable (6% difference upon altering the y^+-value from 108 to 13), the integration over the length of the wire can result in considerable differences for the calculated yarn velocity. This limitation is acceptable for the goal of this study, but should be kept in mind.

As explained in the numerical setup the convergence of the iterations is judged based on a force residual. The influence of the convergence threshold was verified on the coarsest mesh and showed that a threshold of 1e-6 N was sufficient. Additional simulations using a different initial velocity, resulted in nearly the same final velocity,

further validating this statement. Calculations using Sutherland's law for the viscosity were also performed. Compared to the use of a constant viscosity (1.7894e-05 kg/m.s), there was no noteworthy difference and a constant value was thus used.

As was explained during the discussion of the numerical setup, the integration of the wall shear stress over the entire axial length can influence the results. Furthermore, the pressure outlet boundary condition can influence the flow field if it is positioned too close to the nozzle exit. The influence of the axial domain length was investigated by adding an additional 0.2 m to the computational domain. Calculations were performed for a smooth yarn at 3 and 5 bar overpressure. In both cases the domain extension had negligible impact on the results (less than 0.5% on the obtained yarn velocity). No negative axial force was observed as the air velocity still slightly exceeded that of the yarn towards the end of the domain. For hairy yarns slightly negative axial forces might occur but their magnitude and, therefore their influence, can be neglected.

Results for a smooth yarn

Yarn hairiness can severely influence the interaction between the yarn and the flow and as of yet no simple and accurate models are available to incorporate this influence. Therefore, the choice was made to validate the methodology based on smooth yarns, which eliminates parameters related to yarn hairiness from the calculations. For the computations on smooth yarns, the central cylinder is modelled as a moving wall with zero roughness. The feasibility of extending the model to hairy yarns, by assigning a wall roughness to the central cylinder, is investigated later on.

The results for the six different cases involving the polymer coated yarn are listed in Table 5. All calculations started from an estimate of 30 m/s for the yarn velocity. The diameter of the central cylinder was set to 0.21 mm. The air reservoir pressure is referred to as 5 baro for 5 bar gauge pressure and 3 baro for 3 bar gauge pressure.

"[Insert Table 5]"

As can be seen from the table, all calculations were completed in under 5 minutes on 1 processor core (type Intel Xeon E5-2680v3 2.5 GHz). Considering the absence of any tuning and these short calculation times, the accuracy of the calculations can be deemed acceptable. The error relative to the average velocity remains below 5%. From previous research it is also known that the cylindrical nozzles are very sensitive to slight geometrical deviations, consequently the calculation of the flow is less accurate for this nozzle. This was also confirmed by comparing the calculated mass flow rate to experimental values. A separate setup was used to measure the mass flow entering the nozzle through the air inlet (see Figure 1 for definition). For the CON1 nozzle an error of 1% was observed, while the CYL1 nozzle showed a deviation of 3.7%.

Considering only the calculations on the conical nozzles, the correct trend is predicted, configurations resulting in a higher average velocity also have a higher calculated velocity. The methodology, thus, appears to be applicable for optimization of conical nozzles. Most likely, it remains applicable when the scope of the optimization is limited to a parametric variation of a certain base geometry. Validation of the latter statement would, however, require additional experiments.

For the calculations the inlet pressure is set to an average of the measured values at the inlet of the nozzle. The measurement can contain some inaccuracies and, furthermore, the averaging interval to be used is not uniquely defined. This introduces some subjectivity into the results and therefore, the sensitivity of the calculated yarn velocity to the inlet pressure is investigated. Figure 12 shows the calculated yarn velocity for the polymer coated yarn with a linear density of 76.0 tex for absolute inlet pressures ranging from 2 to 6 bar.

"[Insert Figure 12]"

In Figure 12, a sudden change in slope is observed when going from 350 000 to 375 000 Pa. When observing the flow patterns a recirculating flow can be observed on the axis of the tube section at pressures close to 350 000 Pa. This creates a throat section slowing down the supersonic flow and causing it to transition back to subsonic. At 375 000 Pa the recirculation zone is not observable anymore and the flow remains supersonic throughout a larger section of the tube, substantially increasing the force on the yarn. This is illustrated in Figure 13, showing contour plots of axial velocity for both pressure levels.

"[Insert Figure 13]"

Extension to hairy yarns

Approach

Hairiness considerably increases the momentum transfer from the flow to the yarn. In this research an attempt is made to model the yarn hairiness by assigning a wall roughness to the central cylinder. In Fluent wall roughness is implemented by shifting the law of the wall (u^+ versus y^+) downwards over a distance dependent on the dimensionless roughness height (K_s^+).

To avoid problems when large roughness heights are combined with small y^+-values, the y^+-value of a cell is artificially increased by one half of the dimensionless roughness height.

The shift in the law of the wall results in an increased wall shear stress. The corresponding formulas are given below with y^+ and u^+ as defined by Formulas (5) and (6):

$$K_s^+ = (\rho \cdot \sqrt{\frac{\tau_w}{\rho}} \cdot K_s)/\mu \qquad (10)$$

$$u^+ = \frac{1}{\kappa} \cdot \ln\left(\frac{E \cdot (y^+ + K_s^+/2)}{\mu}\right) - \Delta B \quad (11)$$

In these formulas ρ is the density, μ is the dynamic viscosity, τ_w is the wall shear stress, K_s is the physical roughness height, κ is the von Kármán constant (= 0.4187) and E is an empirical constant equal to 9.793. Fluent typically uses y* (which in equilibrium turbulent boundary layers is approximately equal to y^+) in its wall functions instead of y^+ for stability reasons; the dimensionless roughness height and law of the wall are then adapted accordingly. In Formula (11) ΔB is a function dependent on the dimensionless roughness height:

$$\Delta B = 0\ ;\ \text{for } K_s^+ \leq 2.25 \quad (12)$$

$$\Delta B = \frac{1}{\kappa}\ln\left(\frac{K_s^+ - 2.25}{87.75} + C_s K_s^+\right) \cdot \sin\left(0.4258(\ln(K_s^+) - 0.811)\right);\ \text{for } 2.25 < K_s^+ \leq 90 \quad (13)$$

$$\Delta B = \frac{1}{\kappa}\ln(1 + C_s K_s^+)\ ;\ \text{for } K_s^+ > 90 \quad (14)$$

C_s is a roughness constant representing the uniformity of the roughness, for uniform sand grain roughness it is 0.5.

The roughness height for a certain type of yarn is obtained by considering one experiment (e.g. CON1 at 5 bar overpressure propelling a cotton yarn) and tuning the roughness height in the corresponding simulation so that a correct average yarn velocity is calculated. The obtained roughness height is then considered a property of the yarn. The validity of this modelling approach is verified by applying the same roughness height in other simulations (e.g. CON2 at 3 bar overpressure propelling a cotton yarn) and comparing the obtained yarn velocity to the corresponding experiment. As was mentioned in the section on numerical sensitivity, the obtained wall shear stress is not y^+-independent

for the considered resolution. When a wall roughness is applied, the absolute difference between the wall shear stress for different y^+-values also increases. It is, therefore, recommended that simulations concerning hairy yarns are performed on meshes with y^+-values similar to those used for the tuning. It should also be noted that, due to hairiness, the yarn diameter is not uniquely defined. A visual estimate is made based on pictures obtained through a microscope. To assess the influence of the estimated diameter, the roughness tuning is performed and verified for several estimated diameter values.

Tuning the roughness height

The roughness height (RH) was tuned based on the experiment with the CON1 nozzle propelling a 100 tex, cotton yarn at 5 bar overpressure. Based on microscope pictures the yarn diameter (D) was estimated at 0.5 mm. To evaluate the sensitivity with regard to yarn diameter, the roughness tuning was also performed with estimates of 0.4 and 0.6 mm for the diameter. As was done for the polymer coated yarn, the propelled yarn section is weighed after the experiment. Due to the cotton yarn having a lower rigidity, the yarn storage method had to be adapted. Consequently, less yarn was available per experiment. For the case under consideration the inlet pressure was set to 566 855 Pa, the yarn density was determined to be 109.9 Tex. From the experiments an average velocity of 56.2 m/s was determined. Figure 14 shows the variation of calculated yarn velocity with roughness height for several yarn diameters.

"[Insert Figure 14]"

The figure clearly shows that the influence of increasing the roughness height is diminished for high roughness values. This is partly due to the tension force being proportional to the velocity squared but mostly due to the asymptotic behavior of wall shear stress versus roughness height. The values obtained for the roughness heights are 0.19, 0.074 and 0.042 mm for yarn diameters of 0.4, 0.5 and 0.6 mm respectively.

Validation

The diameter-roughness height combinations, obtained from the tuning, are applied to cases using yarn from the same spool but having a different nozzle shape and/or inlet pressure. The specific settings and measurements per case are listed in Table 6 alongside the results from the simulations.

"[Insert Table 6]"

From the results it can be deduced that the initial estimate of the yarn diameter has limited influence on the final result provided that the roughness height was tuned for that specific diameter. The fact that the diameter is not uniquely defined is, thus, of limited importance as long as a reasonable estimate is used.

A relatively large error is observed for the cylindrical nozzle at 5 bar overpressure. As was mentioned previously, the calculation of the flow in a cylindrical nozzle is very sensitive to slight geometric variations. For the cylindrical nozzle at 5 bar overpressure a high backflow was observed. Furthermore, this backflow was found to be rather sensitive to the yarn diameter. Considering the other validation cases with the initial estimate of the diameter (D = 0.5 mm), the results can be deemed acceptable as the error with respect to the average velocity remains below 5% and the correct trend is predicted (cases with a higher experimental velocity also yield a higher simulated velocity). Based on these observations and the fact that the difference between the experiments and the simulations does not increase substantially when considering hairy yarns, it can be concluded that the interaction between a hairy yarn and an airflow can to some extent be simulated by modelling the yarn as a cylinder with an appropriate diameter and accompanying roughness height. It should be noted that no appropriate roughness height will be found when using a too small diameter due to the asymptotic behavior of the wall shear stress with respect to roughness height. On the other hand, using a too large yarn diameter can substantially influence the flow and result in faulty conclusions.

Conclusion

In this research a methodology was developed to quickly estimate the velocity of a yarn as it is propelled by the main nozzle. This was done by incorporating a structural model within the flow solver. The yarn velocity for a single setup can, generally, be obtained in less than 5 minutes on a single processor. The fast calculation allows the algorithm to be used in the context of optimization.

In the simulations the yarn is modelled as a rigid cylinder, allowed to move in the axial direction by assigning it a moving wall boundary condition. The number of cells is kept to a minimum to decrease calculation time at the cost of some accuracy. Calculations are compared to experimentally measured yarn velocities for validation.

The methodology was validated by first considering polymer coated yarns as this avoids the influence of yarn hairiness. From the results it could be deduced that the scope of an optimization, using this method, should be limited to a parametric variation of a selected base geometry. The relative difference between simulated and measured yarn velocity remained below 5%, without any tuning to the simulation setup.

Additionally, an attempt was made to extend the methodology to hairy yarns by assigning a wall roughness to the yarn. The roughness height was tuned based on a single case and, subsequently, applied to other setups for validation. As the yarn diameter of a hairy yarn is not uniquely defined the sensitivity of the results with respect to the diameter estimate was assessed. The results showed that this estimate is not of crucial importance, as long as the roughness height is determined accordingly. Apart from a single case, the error on the calculated velocity remained below 5%. The methodology can thus be extended to hairy yarns by introducing a roughness height at the wall of the cylinder.

The proposed methodology, thus, yields a way of quickly calculating the yarn velocity for smooth yarns launched by a main nozzle based solely on geometrical information and information about the pressure at the inlet. The method has been

extended to hairy yarns by performing a single experiment per yarn type. Care should however be taken when comparing radically different designs or when investigating geometries known to be very sensitive to geometric tolerances.

Funding

This work was supported by the Ghent University Special Research Fund (BOF) [grant number 01D26216].

References

(1) Adanur, S., & Mohamed, M. H. (1992). *Analysis of yarn motion in single-nozzle air-jet filling insertion, Part I: Theoretical models for yarn motion*. The journal of the textile institute, 83, 45-55.

(2) Adanur, S., & Mohamed, M. H. (1992). *Analysis of Yarn Motion in Single-nozzle Air-jet Filling Insertion. Part II: Experimental Validation of the Theoretical Models and Statistical Analysis*. The journal of the textile institute, 83, 56-68.

(3) Adanur, S., & Mohamed, M. H. (1991). *Analysis of yarn tension in air-jet filling insertion*. Textile Research Journal, 61, 259-266.

(4) Adanur, S., & Turel, T. (2004). *Effects of air and yarn characteristics in air-jet filling insertion: Part II: Yarn velocity measurements with a profiled reed*. Textile research journal, 74, 657-661.

(5) Belforte, G., Mattiazzo, G., Viktorov, V., & Visconte, C. (2009). *Numerical Model of an Air-Jet Loom Main Nozzle for Drag Forces Evaluation*. Textile

Research Journal, 79(18), 1664 - 1669.

(6) Chen, L., Feng, Z.-h., Dong, T.-Z., Wang, W.-h., & Liu, S. (2015). *Numerical Simulation of the internal flow field of a new main nozzle in an air-jet loom based on Fluent*. Textile Research Journal, 85(15), 1590 - 1601.

(7) Ishida, M., & Okajima, A. (1994). *Flow Characteristics of the Main Nozzle in an Air-Jet Loom Part I: Measuring Flow in the Main Nozzle*. Textile Research Journal, 64(1), 10-20.

(8) Ishida, M., & Okajima, A. (1994). *Flow Characteristics of the Main Nozzle in an Air-Jet Loom Part II: Measuring High Speed Jet Flows from the Main Nozzle and Weft Drag Forces*. Textile Research Journal, 64(2), 88-100.

(9) Jeong, S. Y., Kim, K. H., Choi, J. H., & Lee, C. K. (2005). *Design of the Main Nozzle with Different Acceleration Tube and Diameter in an Air-Jet Loom*. International Journal of Precision Engineering and Manufacturing 6(1), 23-30.

(10) Jin, Y., Cui, J., Zhu, L., Lin, P., & Hu, X. (2016). *An investigation of some parameter effects on the internal flow characteristics in the main nozzle*. Textile Research Journal, 87(1), 91-101.

(11) Kim, H. D., Lim, C.-M., Lee, H.-J., & Chun, D.-H. (2007). *A Study of the Gas Flow through Air Jet Loom*. Journal of Thermal Science, 16(2), 159–163.

(12) Lan, X., Liu, D., & Feng, Z. (2017). *Structural Optimization of the Main Nozzle in Air-Jet Loom Based on Orthogonal Test Method*. Journal of Textile Engineering & Fashion Technology, 1(5), 00029.

(13) Mohamed, M. H., & Salama, M. (1986). *Mechanics of a Single Nozzle Air-Jet*

Filling Insertion System Part I: Nozzle Design and Performance. Textile Research Journal, 56(11), 683-690.

(14) Moody, L. F. (1944). *Friction Factors for Pipe Flow*. Transactions of the American Society of Mechanical Engineers, 66, 671-681.

(15) Nosraty, H., Jedi, A. A. A., & Mousaloo, Y. (2008). *Simulation analysis of weft yarn motion in single nozzle air-jet loom to study the effective parameters.* Indian journal of Fibre & Textile Research, 33, 45-51.

(16) Oh, T. H., Kim, S. D., & Song, D. J. (2001). A numerical Analysis of Transonic/Supersonic Flows in the Axisymmetric Main Nozle of Air-Jet Loom. Textile Research Journal, 71(9), 783 - 790.

(17) Osman, A. (2017). *Computational Fluid-Structure Interaction Study of the Aeroelastic Behavior of a Wire in Transonic and Supersonic Flows*. (Doctoral dissertation), Ghent University.

(18) Osman, A., Malengier, B., De Meulemeester, S., Peeters, J., Vierendeels, J., & Degroote, J. (2017). *Simulation of air flow-yarn interaction inside the main nozzle of an air jet loom*. Textile Research Journal. Advance online publication. doi: 10.1177/0040517517697646

(19) Prabkeao, C., & Aoki, K. (2005). *Flow Characteristics and Pattern of Main Nozzle of Air Jet Loom*. Paper presented at the Proceedings of the School of Engineering, Tokai University.

(20) Szabó, L., Patkó, I., & Oroszlány, G. (2010). *The dynamic study of the weft insertion of air jet weaving machines.* Acta Polytechnica Hungarica, 7(3), 93-

107.

(21) Uno, M. (1972). *A study on Air-Jet Loom with Substreams Added: Part 4: Length of the Main Nozzle*. Journal of Textile Machinery Society of Japan, 25(7), 72-78.

(22) Uno, M., Yamawaki, K., Ishida, T., Matsui, K., Arakawa, T., Aoyama, H., et al. (1961). *A Study on Air-Jet Looms*. Journal of Textile Machinery Society of Japan, 7(1), 28 - 36.

(23) Wu, Z., Chen, S., Liu, Y., & Hu, X. (2016). *Air-flow characteristics and yarn whipping during start-up stage of air-jet weft insertion*. Textile Research Journal, 86(18), 1988-1999.

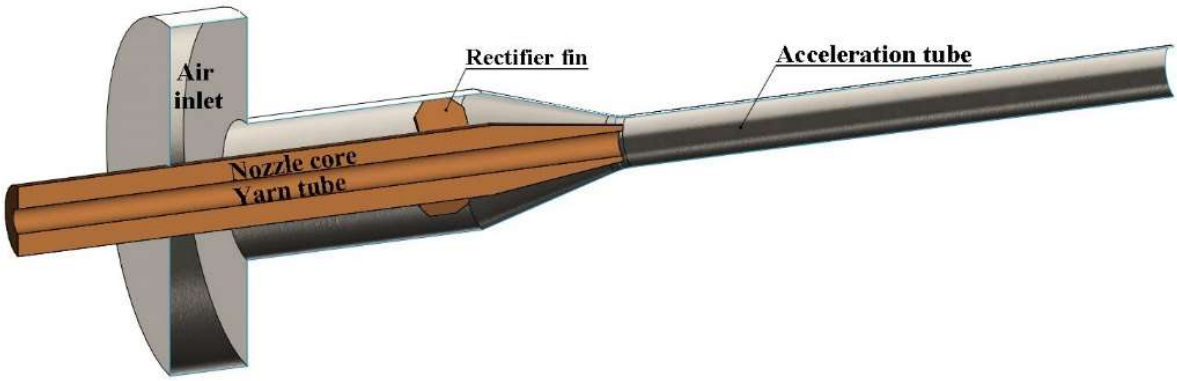

Figure 1: Sketch of a modern main nozzle.

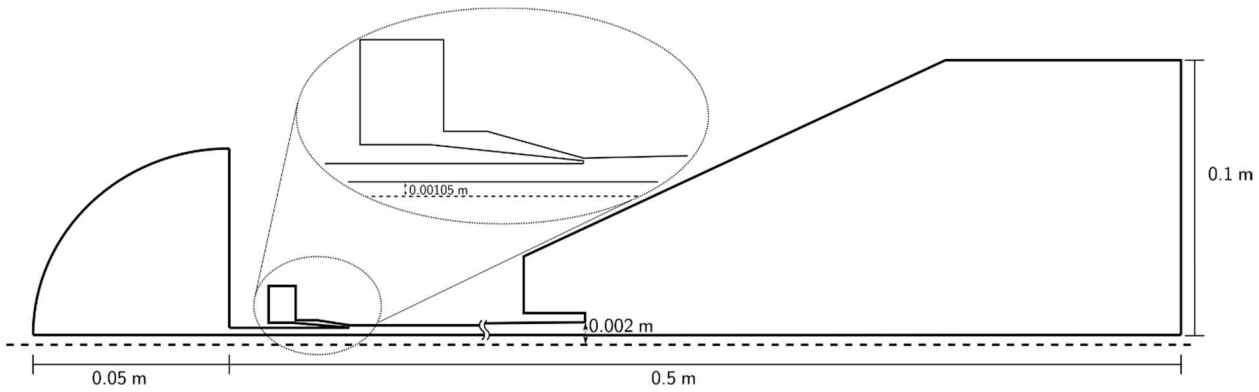

Figure 2: Sketch of an example geometry.

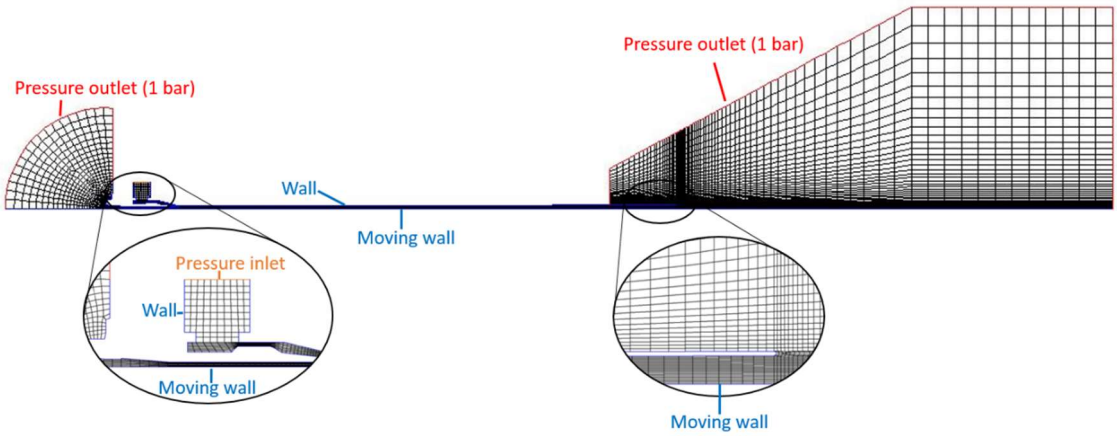

Figure 3: 2D, axisymmetric model of the CON1 nozzle used in the flow simulations.

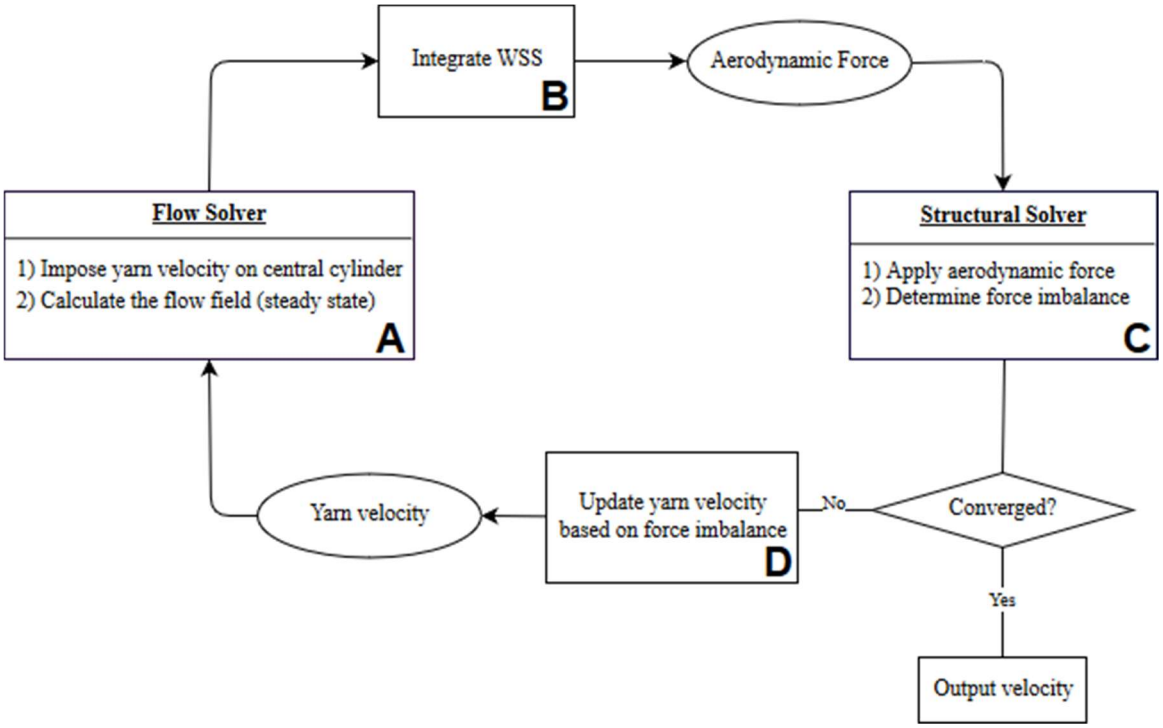

Figure 4: Flowchart of the iterative two-way coupling between the flow solver and a structural calculation.

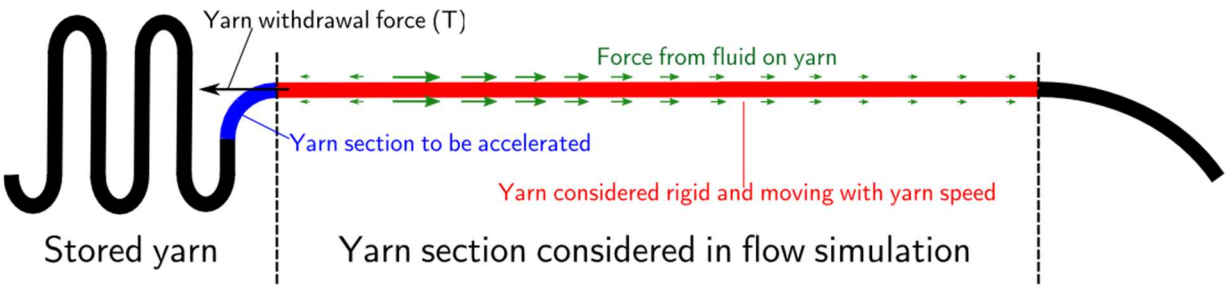

Figure 5: Sketch of the yarn structural model with relevant forces indicated. The section of interest is the red section, which is presumed to be rigid and move at the yarn velocity.

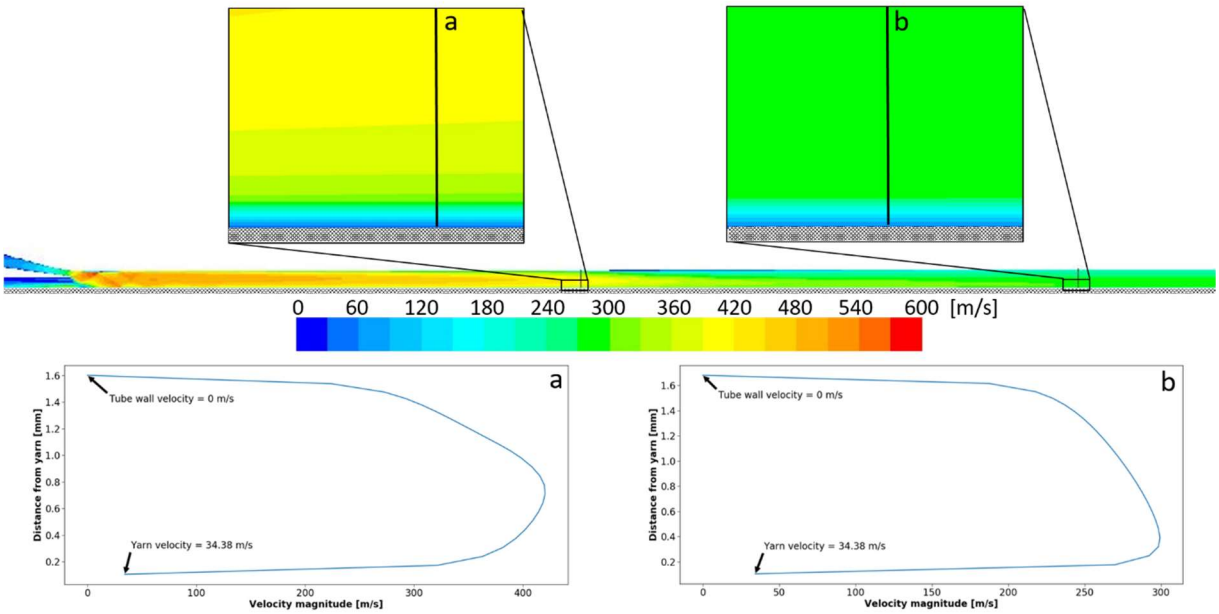

Figure 6: Contour plots showing the calculated velocity magnitude (top) and plots of velocity magnitude along the indicated vertical lines (bottom). The shaded sections represent the yarn. This demonstrates the strong variation of the flow velocity in the axial and radial direction.

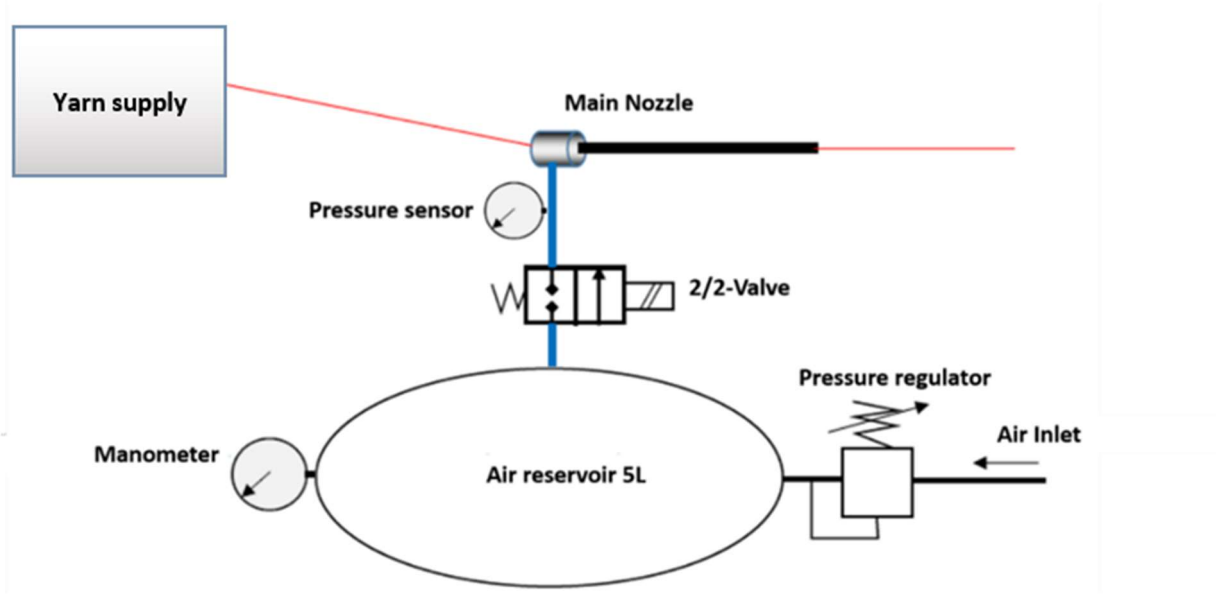

Figure 7: Schematic representation of the experimental setup.

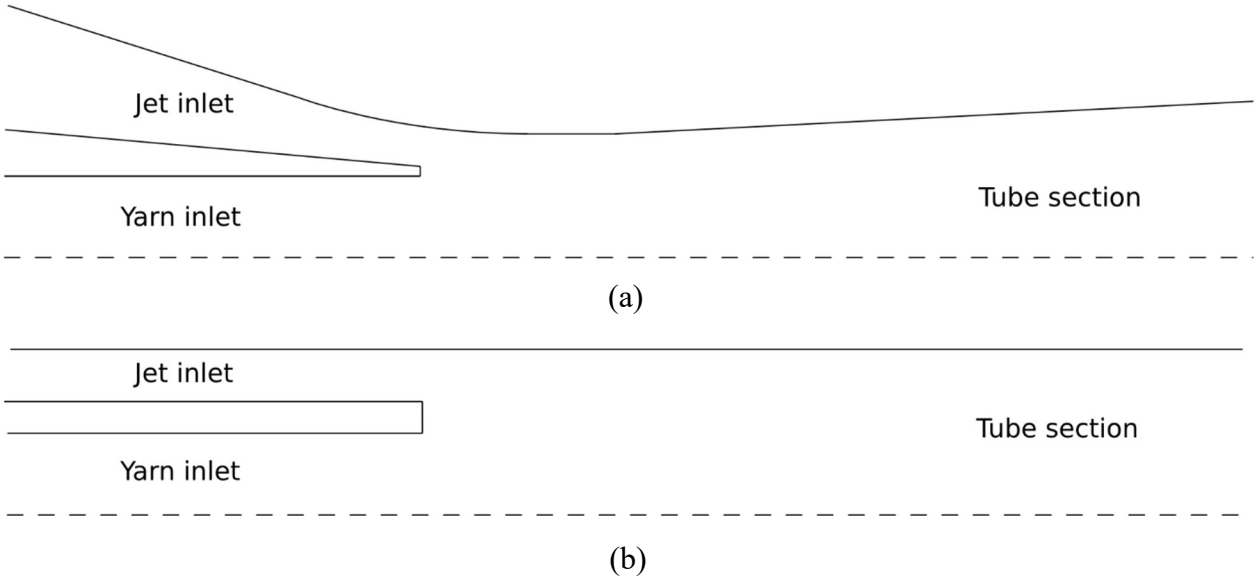

(a)

(b)

Figure 8: Sketch of nozzle geometries. (a) Conical tube and inlet (b) Cylindrical tube and inlet.

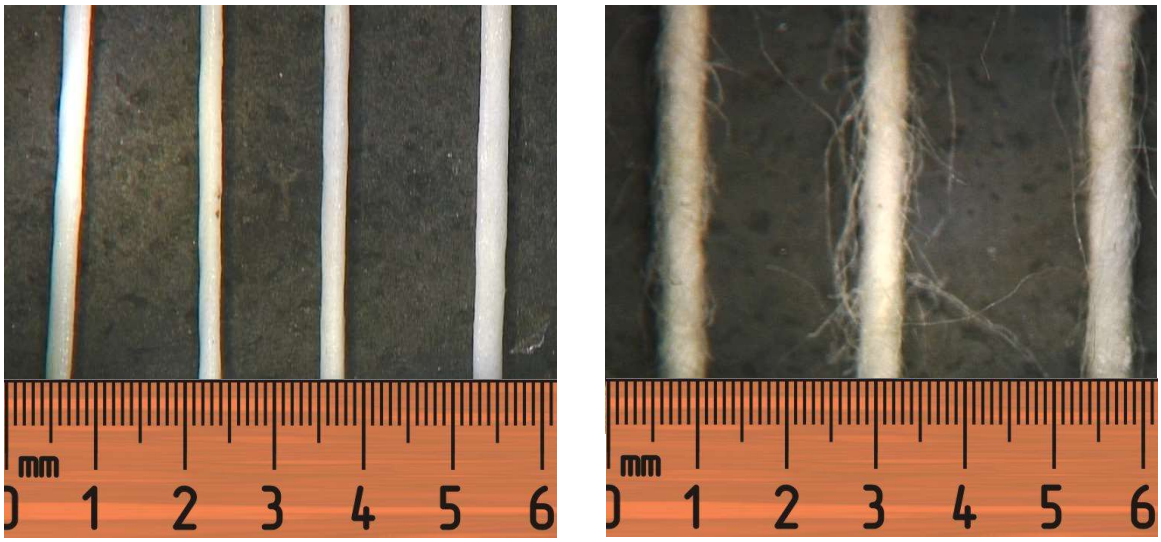

Figure 9: Microscope pictures of a polymer-coated yarn (left) and a cotton yarn (right).

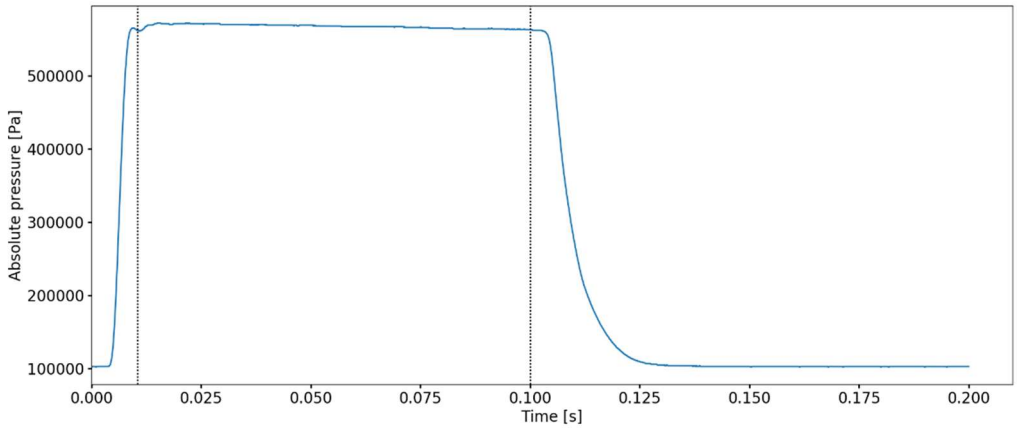

Figure 10: Pressure measured at inlet of CON1 with air reservoir at 5 bar gauge pressure. Dotted lines indicate the accompanying averaging interval.

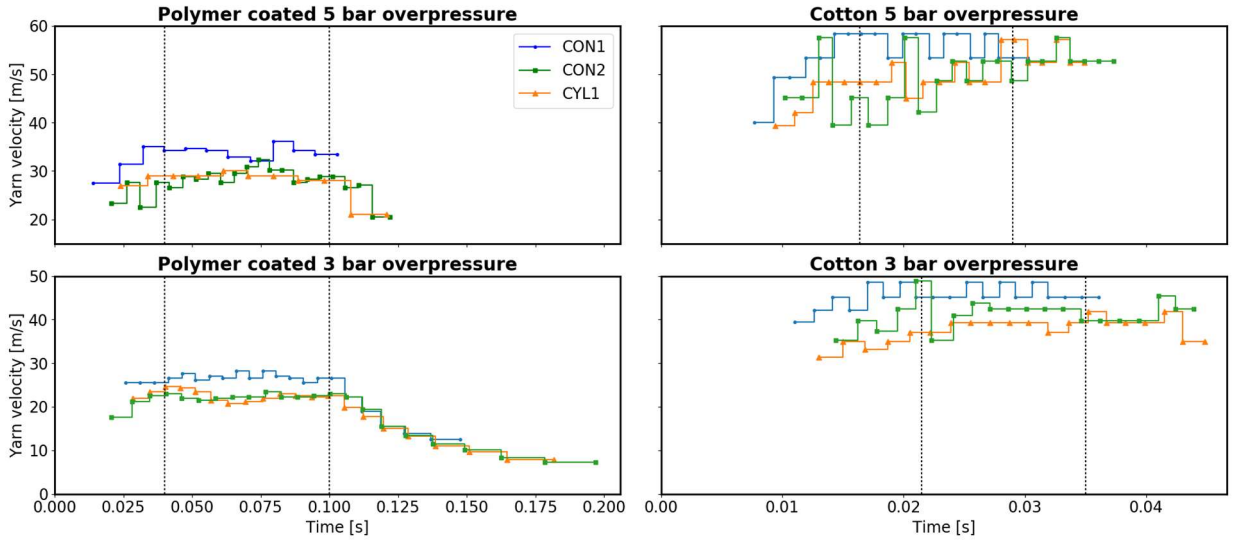

Figure 11: Velocity measurements and the considered regime intervals (in between dotted lines).

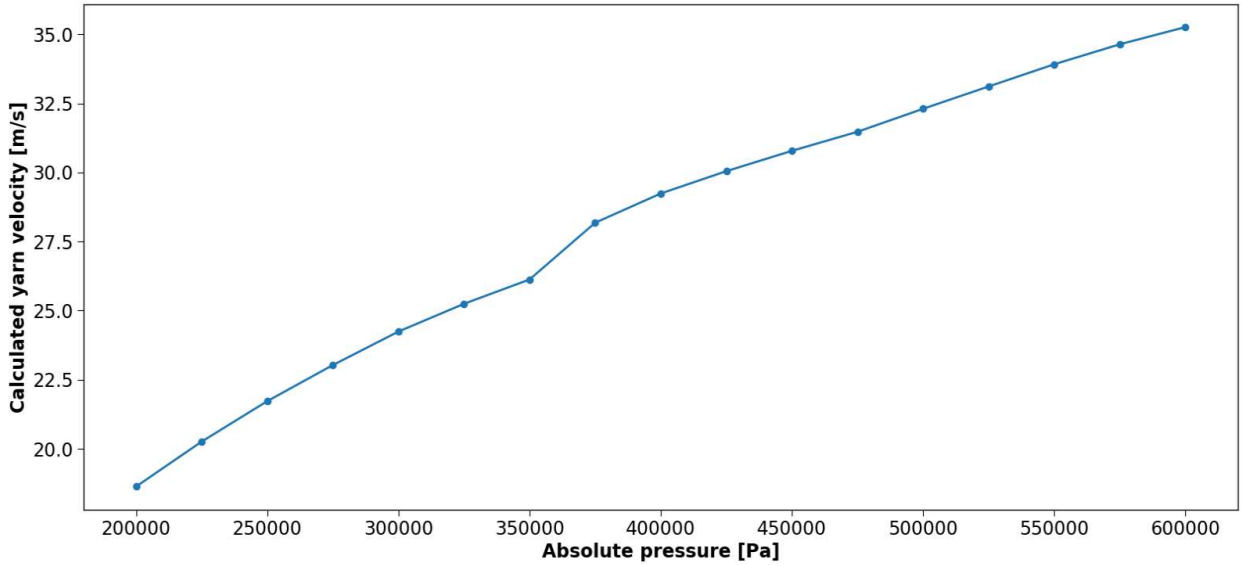

Figure 12: Sensitivity of calculated yarn velocity to inlet pressure for a polymer coated yarn (76 tex) propelled by the CON1 nozzle.

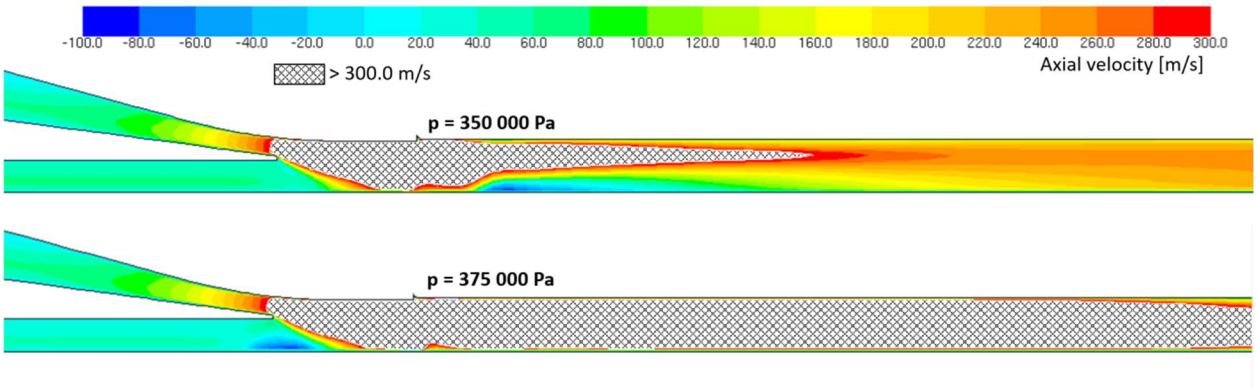

Figure 13: Contour plots of axial velocity at gauge pressures of 350 000 and 375 000 Pa.

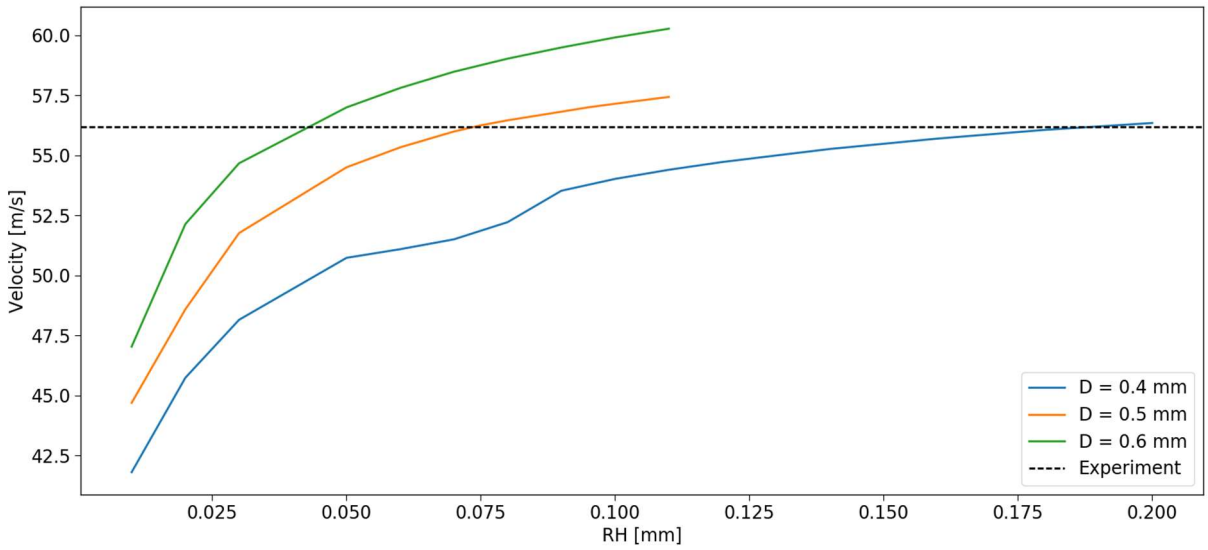

Figure 14: Calculated yarn velocity as a function of roughness height for the CON1 nozzle at 5 bar overpressure for several yarn diameters (D).

Table 1: Geometrical details on the conical nozzles. (α = opening angle of cone ; D = diameter ; A = area ; L = length)

Nozzle type	Converging section			Yarn inlet	Acceleration tube		
	$\alpha_{inner\ cone}$ [°]	$\alpha_{outer\ cone}$ [°]	A_{throat} [mm^2]	D [mm]	L [mm]	D_{start} [mm]	D_{end} [mm]
CON1	15	29	4.8	2.5	243.0	3.0	4.0
CON2	10	22	3.8	2.9	242	3.5	4.0

Table 2: Experimental values at 5 bar overpressure. Minimum and maximum velocity are those observed in the considered regime interval.

Nozzle	Yarn	Average pressure [Pa]	Minimum velocity [m/s]	Maximum Velocity [m/s]	Average Velocity [m/s]	Error [m/s]
CON1	PC	566855	32.1	36.1	33.9	± 0.09
CON1	C		53.4	58.3	56.2	± 0.49
CON2	PC	573630	26.6	32.4	29.1	± 0.09
CON2	C		39.5	57.5	48.1	± 0.47
CYL1	PC	579098	28.0	30.0	29.0	± 0.09
CYL1	C		45.0	57.2	49.5	± 0.48

Table 3: Experimental values at 3 bar overpressure. Minimum and maximum velocity are those observed in the considered regime interval.

Nozzle	Yarn	Average pressure [Pa]	Minimum velocity [m/s]	Maximum Velocity [m/s]	Average Velocity [m/s]	Error [m/s]
CON1	PC	374924	25.6	28.3	26.9	± 0.09
CON1	C		45.1	48.6	46.1	± 0.44
CON2	PC	385940	21.5	23.4	22.4	± 0.09
CON2	C		35.3	48.9	41.8	± 0.43
CYL1	PC	369694	20.8	24.7	22.5	± 0.09
CYL1	C		37.0	39.3	38.6	± 0.43

Table 4: Mesh sensitivity analysis on the CON1 nozzle at 5 bar overpressure.

# Cells	Force [N]	Velocity [m/s]
9733	0.09016	34.17
38932	0.09037	34.21
155728	0.08852	33.86
622912	0.08990	34.13

Table 5: Results of the calculations concerning the polymer coated yarn.

Case	ρ_A [tex]	Minimum velocity [m/s]	Maximum Velocity [m/s]	Average Velocity [m/s]	Calculated Velocity [m/s]	Calculation time [hh:mm:ss]
CON1, 5 baro	76.0	32.1	36.1	33.9	34.4	00:03:27
CON1, 3 baro	77.3	25.6	28.3	26.9	27.9	00:04:04
CON2, 5 baro	77.4	26.6	32.4	29.1	28.5	00:04:22
CON2, 3 baro	77.2	21.5	23.4	22.4	23.5	00:03:48
CYL1, 5 baro	76.3	28.0	30.0	29.0	27.6	00:04:03
CYL1, 3 baro	76.3	20.8	24.7	22.5	22.1	00:04:36

Table 6: Results of the validation cases for hairy yarns. Roughness height was tuned on the CON1, 5 baro case.

Case	ρ_A [tex]	Average experimental velocity [m/s]	Simulated velocity [m/s] For given (D [mm] ; RH [mm])		
			(0.4 ; 0.19)	(0.5 ; 0.074)	(0.6 ; 0.042)
CON1, 5 baro	109.9	56.2	56.2	56.2	56.2
CON1, 3 baro	99.3	46.1	46.6	46.6	46.7
CON2, 5 baro	103.0	48.1	47.9	47.9	48.1
CON2, 3 baro	106.0	41.8	40.2	40.0	39.8
CYL1, 5 baro	105.4	49.5	44.7	45.4	45.7
CYL1, 3 baro	99.1	38.6	38.0	38.2	38.3